HHS Public Access

Author manuscript

Oncogene. Author manuscript; available in PMC 2024 February 01.

Published in final edited form as:

Oncogene. 2023 August ; 42(32): 2428–2438. doi:10.1038/s41388-023-02759-7.

Androgen-regulated stromal complement component 7 (C7) suppresses prostate cancer growth

Zhicheng Zhou[1,6], **Deyong Jia**[1,6], **Ohjoon Kwon**[1], **Shan Li**[2], **Huiyun Sun**[2], **Martine P. Roudier**[1], **Daniel W. Lin**[1], **Lawrence True**[3], **Colm Morrissey**[1], **Chad J. Creighton**[4], **John K. Lee**[2], **Li Xin**[1,5,✉]

[1]Department of Urology, University of Washington, Seattle, WA, USA.

[2]Division of Human Biology, Fred Hutchinson Cancer Research Center, Seattle, WA, USA.

[3]Department of Laboratory Medicine and Pathology, University of Washington, Seattle, WA, USA.

[4]Dan L. Duncan Comprehensive Cancer Center, Baylor College of Medicine, Houston, TX, USA.

[5]Institute of Stem Cell and Regenerative Medicine, University of Washington, Seattle, WA, USA.

[6]These authors contributed equally: Zhicheng Zhou, Deyong Jia.

Abstract

The complement system is a major component of the innate immune system that works through the cytolytic effect of the membrane attack complex (MAC). Complement component 7 (C7) is essential for MAC assembly and its precisely regulated expression level is crucial for the cytolytic activity of MAC. We show that *C7* is specifically expressed by the stromal cells in both mouse and human prostates. The expression level of *C7* inversely correlates with clinical outcomes in prostate cancer. *C7* is positively regulated by androgen signaling in the mouse prostate stromal cells. The androgen receptor directly transcriptionally regulates the mouse and human *C7*. Increasing C7 expression in the C57Bl/6 syngeneic RM-1 and *Pten-Kras* allografts suppresses tumor growth in vivo. Conversely, *C7* haploinsufficiency promotes tumor growth in the transgenic adenocarcinoma of the mouse prostate (TRAMP) model. Interestingly, replenishing C7 in androgen-sensitive *Pten-Kras* tumors during androgen depletion only slightly enhances cellular apoptosis, highlighting the diverse mechanisms employed by tumors to counteract complement activity. Collectively, our research indicates that augmenting complement activity could be a promising therapeutic approach to impede the development of castration resistance in prostate cancer.

✉**Correspondence** and requests for materials should be addressed to Li Xin. xin18@uw.edu.

AUTHOR CONTRIBUTIONS

Conceptualization, LX and ZZ; Investigation, ZZ, DJ, OK, SL, HS, and MR; Formal analysis: ZZ, MR, CJC, and LX; Writing, LX, CJC, and ZZ; Resources, DL, LT, and CM; Funding Acquisition, LX and JKL; Supervision, LX and JKL.

COMPETING INTERESTS

The authors declare no competing interests.

ADDITIONAL INFORMATION

Supplementary information The online version contains supplementary material available at https://doi.org/10.1038/s41388-023-02759-7.

INTRODUCTION

Prostate cancer responds to antiandrogen therapies but often recurs and becomes castration resistant prostate cancer (CRPC) [1]. It is important to comprehensively understand the underlying mechanisms to develop novel therapeutic strategies for CRPC.

The complement system is a major component of the innate immune system that enhances the ability of antibodies and phagocytic cells to clear foreign pathogens and damaged cells, promote inflammation, and attack the pathogen's cell membrane. The system consists of a cascade of plasma serine proteases and membrane proteins [2]. Complement activation involves multiple tightly regulated steps that can be defined into three pathways including the classic pathway activated via antigen-antibody complexes, the lectin pathway via binding of pattern-recognizing mannose-binding lectins, and the alternate pathway via other permissive surfaces. Formation of the C3 convertase and C5 convertase complexes are common downstream events in all three activation pathways. Activation leads to the generation of an opsonin (C3b) that marks cells or cell debris for phagocytosis by macrophages and two potent anaphylatoxins (C3a and C5a) that recruit neutrophils to areas of tissue damage and inflammation. The final step of complement activation is the membrane-anchorage of the terminal complement complex C5b9 which consists of C5b, C6, C7, C8, and C9 proteins. The anchored complex is called the membrane attack complex (MAC). The MAC destroys membrane integrity, causing calcium influx and cell lysis [2].

The complement system is not only an important part of the innate immune response to invading pathogens, but also plays critical roles in cancer progression. Complement can be activated in response to natural IgM antibodies against tumor antigens and therapeutic monoclonal antibodies, or via direct cleavage of C3 and C5 by tumor derived proteases such as PSA in prostate cancer [3]. Although some upstream players in the complement system such as C3a and C5a can mediate pro-tumorigenic effects [4, 5], the final step of complement activation, i.e. MAC accumulation on tumor cells, leads to cancer cell lysis and is thereby considered detrimental to cancer cells. Not surprisingly, cancer cells have developed diverse mechanisms to antagonize the final activation of the MAC activity including the expression of negative regulators such as CD55 and clusterin as well as downregulation of the terminal complex components [6–10].

C7 is an essential protein to anchor and insert MAC into the cell membrane through its hydrophobic site. Interestingly, it is the only late C component that is not predominantly synthesized by hepatocytes but is expressed by specific cell lineages throughout the body such as the endothelial and fibroblast cells [11, 12]. This expression pattern probably reflects a regulatory mechanism restricting MAC assembly at local tissues. Insufficient C7 will limit MAC assembly. Additionally, when the number of MAC on the membrane of targeted cells is inadequate, it (sublytic MAC) does not cause cell lysis but instead activates PI3K and ERK signaling via a G_i-dependent manner and promotes inflammation by activating inflammasome [13, 14]. In addition, insufficient C7 will also attenuate efficient anchorage of C5b-9 into the membrane of targeted cells and cause the formation of cytolytically inactive soluble C5b-9 complex (sC5b-9). SC5b-9 can promote inflammatory responses by upregulating cytokines and adhesion molecules [15]. Signaling mediated by the sublytic

MAC and SC5b-9 are both pro-tumorigenic. Therefore, a precisely regulated C7 expression level is critical for the cytolytic anti-tumor activity of MAC. Functionally defective genetic variants of C7 are associated with cancer susceptibility [16] and C7 expression has been shown to be decreased in some types of cancers [17], but the functional significance of this reduction remains unknown. In this study, we interrogated the cellular source of C7 in prostate tissues, investigated how C7 expression is regulated, and determined how its expression level affects prostate cancer progression and development of therapeutic resistance.

RESULTS

The stromal cells are the major source of *C7* in the prostate

C7 is the only complement component that is not predominantly synthesized by hepatocytes. Therefore, locally produced C7 is a limiting factor for the formation and function of the terminal membrane attack complex (MAC) in individual tissues. Consistently, qRT-PCR analysis shows that *C3* is highly expressed in the mouse liver whereas *C7* is expressed at a higher level in the mouse prostate than liver (Supplementary Fig. 1A, B), indicating that the complement system is a unique component in the prostate tissue microenvironment. Expression of the complement components in mouse and human prostate stroma has been reported previously [18–20]. We sought to determine the major cellular source of C7 in the mouse prostate. QRT-PCR analysis shows that *C7* is almost exclusively expressed by the prostate stromal cells (Fig. 1A and Supplementary Fig. 1C, D). Previously, we defined three major stromal subpopulations in the mouse prostate: the growth factor-expressing Sca-1^{+}CD90^{+} cells, the Sca-1^{+}CD90$^{-/low}$ cells that express inflammatory factors, and the Sca-1^{-}CD90^{+} smooth muscle cells [19]. QRT-PCR analysis shows that the Sca-1^{+}CD90$^{-/low}$ stromal cells are the major source of both *C7* and *C3* (Fig. 1B and Supplementary Fig. 1E), which is consistent with the putative role of this cell population in defense, immune responses, and tissue repair. Our previous study also showed that the stromal cells in the mouse proximal prostatic ducts near the urethra are phenotypically distinct from those in the non-proximal (distal) prostatic ducts [21–23]. We FACS-isolated the prostate stromal cells in the proximal and distal mouse prostate tissues and examined the expression of *C7*. Figure 1C shows that *C7* expression in the proximal prostatic stromal cells is approximately 2.57-fold of that in the distal prostatic ducts.

In the human prostate, *C7* is also exclusively expressed by the stromal cells (Fig. 1D and Supplementary Fig. 1F, G). We showed previously that the stromal cells in the mouse proximal prostate share molecular features with those of human periurethral transition zone prostate [21, 23]. QRT-PCR analysis shows that the *C7* expression in the transition zone prostate stromal cells is approximately 5.44-fold of that in peripheral zone (Fig. 1E), which is consistent with the observation from a single cell RNA-seq analysis [20]. Collectively, these results show that the stromal cells are the major cellular source of *C7* in the prostate. The similar anatomy-associated expression pattern of *C7* in mouse and human further corroborates our previous reports that the mouse and human prostates shared some anatomy-associated molecular features [22, 24].

Of note, we attempted to examine the expression of C7 by Western Blot and immunostaining. However, two of the commercially available antibodies (ab126786 and ab192346 from Abcam) that we tried could not differentiate the expression levels of C7 in wild type and *C7* knockout mouse tissues, indicating that they are not specific (Supplementary Fig. 1H). Therefore, we were not able to verify C7 expression at the protein level throughout this study.

The expression level of C7 inversely correlates with clinical outcome of prostate cancer

Analysis of multiple human prostate cancer genomic datasets reveals that the expression of *C7* was decreased significantly in human prostate cancer specimens as compared to normal prostate tissues (Fig. 2A) and the expression was further decreased in metastatic prostate cancer specimens (Fig. 2B). In addition, *C7* expression is lower in specimens with higher Gleason scores (Fig. 2C) and in early metastasis after rising PSA (Fig. 2D). A lower *C7* expression is also associated with early biochemical recurrence (Fig. 2E). In silico analysis cannot distinguish a lower expression level of *C7* from a lower stromal composition in the tumors. Therefore, we laser captured the stromal cells from human prostate cancer specimens of different Gleason patterns and adjacent normal tissues collected through the University of Washington Biorepository Program and determined the expression of *C7* using qRT-PCR. Figure 2F corroborates that the stromal *C7* expression is decreased in the stroma of prostate cancer.

It should be noted that the association of C7 expression with time to adverse outcome is not statistically significant in two other prostate cancer datasets [25, 26], though the Taylor dataset showed a significant correlation of C7 expression with Gleason grade. Associating gene expression with time to adverse event in prostate cancer patients is difficult with the limited public gene expression datasets available, as much longer follow-up time to cancer-specific death (~10 years) would ideally be needed here. Unfortunately, available datasets have much more limited follow-up and would rely on endpoint surrogates like biochemical recurrence. Nevertheless, observing associations of C7 with more aggressive cancers in multiple independent studies considerably strengthens this finding.

C7 is positively regulated by the androgen receptor in the prostate stromal cells

The expression of *C7* was significantly downregulated in the prostate stromal cells of castrated mice (Fig. 3A), suggesting that its expression is regulated by androgen signaling. Culturing the embryonic urogenital sinus mesenchymal cells (Fig. 3B) or adult mouse prostate stromal cells (Fig. 3C) in charcoal-striped serum downregulated *C7*. Supplementing dihydrotestosterone restored the expression of *C7* (Fig. 3B, C). Consistently, overexpressing the androgen receptor (AR) in the in vitro cultured primary mouse prostate stromal cells upregulated *C7* (Fig. 3D and Supplementary Fig. 2). To further corroborate the regulation of *C7* by AR in vivo, we treated adult *Col1a2-CreER^{T2};AR$^{flox/Y}$* bigenic mice with tamoxifen to disrupt AR in the prostate stromal cells. Figure 3E confirms that ablating *AR* in the prostate stromal cells reduced the expression of *C7*. These results demonstrate that AR positively regulates *C7* in the mouse prostate stromal cells.

To determine whether the expression of *C7* in human prostate is also regulated by androgen signaling, we utilized an in vitro prostate cancer tissue slice culture (TSC) [27]. As shown in Fig. 3F, prostate cancer specimens and adjacent benign tissues obtained from patients who had undergone radical prostatectomy were cut into 200–500 μm slices using a vibratome and cultured in a well insert that was partially submerged in media and exposed to atmospheric oxygen. The tissue architecture and diverse cell populations in the TSCs are maintained during the culture [27]. We performed TSC in the presence and absence of enzalutamide, a potent androgen receptor inhibitor. Figure 3F shows that enzalutamide treatment significantly reduced the expression of *C7* in the FACS-isolated stromal cells in the cultured tissue slices from both cancerous and benign tissues. Of note, stromal cells in the tumor specimens expressed *C7* at a much lower level than those from the benign tissues, which corroborates the result shown in Fig. 2F. Collectively, these results show that *C7* is regulated by androgen signaling in both the human and mouse prostate stromal cells.

We examined the 2 kb genomic sequence upstream of the transcription start sites of the mouse and human C7 and identified 4 and 2 non-classical androgen-responding element (ARE) sites (TGTTCT) in the mouse and human *C7* promoter, respectively (Fig. 3G, H). We disrupted the ARE sites by site-directed mutagenesis and cloned the wild type and mutated 2 kb human and mouse genomic fragments into a luciferase promoter reporter plasmid. Overexpressing AR upregulated transcriptional activity of wildtype human and mouse *C7* in WPMY and mouse prostate stromal cells, respectively, but had no effect on the mutant reporters (Fig. 3G, H). ChIP assay shows that AR directly binds to most of these sites (Fig. 3I, J). These results support direct transcriptional activation of *C7* by AR.

C7 suppresses mouse prostate cancer growth in vivo

To determine how expression of *C7* affects prostate cancer growth in vivo, we infected the C57BL/6 syngeneic RM-1 prostate cancer cells with a lentivirus expressing C7 and the control empty lentivirus (Supplementary Fig. 3A). Infected cells were transplanted subcutaneously in male C57BL/6 host mice. Figure 4A shows that overexpressing C7 suppressed the growth of RM-1 tumors by 62.8% in tumor weight. Immunostaining of BrdU and the cleaved caspase 3 revealed a very slight decrease in cell proliferation but a prominent increase in cell apoptosis (Fig. 4B, C). C7 overexpression also suppressed subcutaneous tumor growth of the *Pten-Kras* C57BL/6 syngeneic mouse prostate cancer cell line [23] by 32.7% (Fig. 4D and Supplementary Fig. 3B), reduced cell proliferation (Fig. 4E), and enhanced cell apoptosis (Fig. 4F), indicating that the C7-mediated tumor suppressive effect is not restricted to specific tumor models. Of note, C7 overexpression did not significantly suppress the growth of RM-1 or *Pten-Kras* in vitro within 3 days of culture (Supplementary Fig. 3C). To corroborate that C7 overexpression enhanced the formation of the membrane attack complex, we took advantage of the WU13-15 monoclonal antibody. This antibody recognizes a neoepitope on complement C9 protein only if it is integrated in the terminal complement complex. Our result confirmed that the staining intensity of WU13-15 is elevated in the RM-1 tumors overexpressing C7 (Supplementary Fig. 3D).

C7 is produced by the stromal cells in the prostate. To recapitulate the situation more faithfully, we mixed the control and C7-overexpressing C57BL/6 mouse prostate stromal

cells with prostate cancer cells and transplanted the cell mixtures subcutaneously in male C57BL/6 host mice. Coculturing with C7-expressing mouse prostate stromal cells also suppressed the growth of both RM-1 (Fig. 4G) and *Pten-Kras* (Fig. 4H), but the suppressive effect was relatively minor as compared to that caused by cancer cell-autonomous expression of C7. This is likely because the stromal cells were substantially diluted along the growth of the tumors in the coculture model so that the expression level of C7 in the coculture models was much lower than that in the tumor cells only models in Fig. 4A and D. Nevertheless, immunostaining of the cleaved caspase 3 (CC3) corroborated an increase in cell apoptosis in the C7-expressing groups (Fig. 4I, J). These studies show that elevated complement activity can suppress the growth of the allograft models of mouse prostate cancers.

We sought to further corroborate the role of C7 in prostate cancer growth using a mouse model for autochthonous prostate cancer. *C7* heterozygosity reduces the expression of *C7* by half but does not affect prostate development or homeostasis as shown by normal prostate size, histology, and expression patterns of lineage markers (Supplementary Fig. 4A–D). We generated a cohort of *TRAMP* and *TRAMP;C7*$^{+/-}$ mice on a pure C57BL/6 background. Figure 5A shows that the mean tumor weight of the 22-wk-old *TRAMP;C7*$^{+/-}$ mice was 1.46-fold of that of the age-matched *TRAMP* mice. H&E staining shows that the prostates from both groups uniformly and diffusely displayed invasive adenocarcinomas in the dorsal and anterior lobes (Fig. 5B). We evaluated and scored the histology of the tumors based on the published Bernam-Booty scoring system [28]. Median adjusted scores of the control and *TRAMP;C7*$^{+/-}$ mouse prostate cancers were 449 and 534, but were not statistically different (Fig. 5B). Immunostaining shows a reduction of staining intensity for C5b-9 in the *TRAMP;C7*$^{+/-}$ mouse prostate than in the control TRAMP prostate tissues (Supplementary Fig. 4E). In the *TRAMP;C7*$^{+/-}$ mouse prostates, the proliferating index was 1.62-fold of that in the control TRAMP group (Fig. 5C). Western blot analysis of expression of the cleaved caspase 3 indicated that the apoptotic index was reduced in the *TRAMP;C7*$^{+/-}$ mouse prostate (Fig. 5D). Collectively, these studies demonstrate that C7 suppresses prostate cancer growth of the TRAMP model, although the overall histological progression is not significantly delayed.

C7 potentially cooperates with androgen deprivation to promote cellular apoptosis

We showed that androgen deprivation downregulated *C7*. Therefore, the complement activity within the prostate tissue could be attenuated upon androgen deprivation. We sought to investigate whether restoring C7 during androgen deprivation further suppressed tumor cell survival and growth. As the endogenous expression of C7 in prostate stromal cells was significantly reduced upon castration, we would not be able to reach a conclusion by comparing the response of tumor cells in the *TRAMP* and *TRAMP;C7*$^{+/-}$ mice to castration. Instead, we took advantage of the castration sensitive *Pten/Kras* syngeneic tumor model. A better disease-relevant approach would be coculturing the *Pten/Kras* tumor cells with prostate stromal cells that express exogenous C7. However, the local expression of C7 is difficult to sustain in this setting because the stromal cells would be quickly diluted in the fast-growing *Pten/Kras* model. Therefore, we opted to engineer the *Pten/Kras* cells to express doxycycline regulatable C7 (Supplementary Fig. 5A). The $\Delta Ct^{(C7\text{-}Gapdh)}$ values

of the control and doxycycline treated Pten/Kras cells were 11.52 and 9.59, respectively. In comparison, the $\Delta Ct^{(C7\text{-}Gapdh)}$ values of total mouse prostate cells and FACS-sorted mouse stromal cells were 8.2 and 1.73, respectively. Therefore, the doxycycline-induced overexpression level is comparable to that of mouse prostates and is physiologically relevant. The cells were transplanted subcutaneously in male C57BL/6 mice. As shown in Fig. 6A, once the tumors were established, the hosts were randomly divided into 2 groups and were either castrated or underwent sham surgery. A day later, each group was further divided into 2 groups and fed with and without doxycycline-containing water, respectively, to manipulate the C7 expression. Mice were collected at either 1 week or 4 weeks after castration to evaluate tumor cell survival and growth.

There was no significant difference in tumor weight or tumor cell proliferation among the groups at one week after castration or sham surgery (Fig. 6B and Supplementary Fig. 5B, C). Castration or induction of C7 expression induced cell apoptosis and the apoptotic index was further increased in the group with both castration and C7 induction (Fig. 6C) but did not reach statistical significance based on the two-way ANOVA analysis. Figure 6D shows that castration or C7 expression significantly reduced tumor weight 4 weeks later. The average tumor weight was further reduced in the group with both castration and C7 expression in 2 independent experiments, but the reduction did not reach statistical significance, either. Immunostaining of BrdU showed a comparable reduction of proliferating indices among the groups (Fig. 6E). Western blot analysis of the cleaved caspase 3 indicated a trend towards increased cell apoptosis when C7 expression and castration happened simultaneously (Fig. 6F), though the increase was not statistically significant possibly due to a large variation in signaling intensity. The results suggest that upregulating C7 expression has the potential to enhance apoptosis in prostate cancer cells undergoing androgen deprivation. The result also suggests that upregulating C7 alone may not be sufficient to enhance the complement activity because cancer cells have been shown to employ diverse mechanisms to undermine the complement activity [6–10].

DISCUSSION

Prostate cancer inevitably develops resistance to anti-androgen therapies and becomes castration resistant. Various underlying mechanisms have been identified, including amplification, mutations, and alternative splicing of the androgen receptor, activation of signaling mediated by other nuclear receptors and kinases, and the more recently discovered treatment-induced lineage plasticity [1, 29]. Our study reveals that reducing the cytolytic activity of the complement system is another potential mechanism that contributes to the development of castration resistance.

Tumor cells have been shown to develop various mechanisms to inhibit the formation of the MAC. For example, cancer cells express a high level of clusterin, which can bind to the nascent amphiphilic C5b-9 complex, making it cytolytically inactive soluble C5b-9 [9]. In addition, cancer cells also express CD59, which inhibits formation of C5b-9 by blocking C9 polymerization [10]. Our study shows that the expression of C7 in the tumor stroma is significantly lower than that in normal prostate stroma. In addition, ablating androgen receptor signaling further downregulates C7. These observations establish the

downregulation of C7 as another mechanism through which tumors prevent the formation of MAC and suggest that boosting the cytolytic activity of the complement system can help restrain castration resistance. On the other hand, due to these multiple parallel mechanisms that tumors have developed to inhibit the MAC formation, it is possible that addition of C7 alone is not enough to fully restore the MAC activity and improve the therapeutic efficacy of anti-androgens. For example, our result shown in Fig. 6D shows that increasing C7 only caused a minor decrease in tumor weight. Combining anti-CD59 or Custirsen, an antisense oligonucleotide against clusterin, with C7 may further enhance the therapeutic efficacy of enzalutamide.

We also show that C7 is expressed at a higher level in the stroma in the transition zone (TZ) than in those of peripheral zone (PZ). How this regional specific expression pattern of C7 is established remains unclear. An early study shows the existence of cis elements for C/EBPα, AP1, HNF3, and NF1 in the C7 promoter [30]. It is possible that TZ stromal cells exhibit intrinsically higher expression or activities of these transcription factors, leading to a higher C7 expression level. Alternatively, the higher C7 expression may reflect a response of TZ stroma to physiological or pathological stimuli. In either scenario, this region-specific differential expression pattern is reflective of the anti-microbial function of the complement system. The transition zone glands are anatomically closer to the urethra [31], thereby more susceptible to bacterial prostatitis potentially caused by urine reflux [32]. A higher complement activity in TZ may help guard an aseptic environment in the prostate by quickly eradicating pathogenic microbes. We showed that AR can directly transcriptionally regulate C7. SRD5A2, an enzyme critical for the biogenesis of dihydrotestosterone, is highly expressed in stromal cells in the mouse proximal prostate and human transition zone [19, 20, 22]. This may lead to a relatively higher testosterone level in these regions and contribute to the higher C7 expression. An AR binding peak was not identified at the *C7* locus in a genome-wide AR ChIP-Seq analysis in prostate fibroblast cells [33]. This is probably because the binding is weak when androgen levels and androgen receptor expression are low. In our in vitro ChIP assay, AR expression could boost C7 promoter activity by 20–60%. AR has been reported to interact with C/EBPα to activate transcription [34] and AP1 motif was found to be enriched in the AR cistrome in prostate fibroblast cells [35] and inflamed epithelial cells [36]. Therefore, AR may also regulate the expression of C7 through interaction with these transcription factors. A comprehensive understanding of how C7 is regulated will inspire additional therapeutic strategies to boost MAC activity and constrain the development of castration resistance.

MATERIALS AND METHODS

Mice

All animals used in this study received humane care in compliance with the principles stated in the Guide for the Care and Use of Laboratory Animals, NIH Publication, 1996 edition, and the protocol was approved by the Institutional Animal Care Committees of University of Washington. The C57BL/6 mice were purchased from Charles River (Wilmington, MA). *Col1a2-CreER*^{T2}, *C57BL/6-Tg(TRAMP)8247Ng/J*, and *C57BL/6N-C7em1(IMPC)J/J* mice were purchased from the Jackson Laboratory (Bar Harbor, ME). The *AR*$^{f/Y}$ mice were from

Drs. Guido Verhoeven and Karel De Gendt at the Catholic University of Leuven in Belgium [37]. All mice were on the C57BL/6 background. Mice were genotyped by polymerase chain reaction using mouse genomic DNA from tail biopsy specimens. The sequences of genotyping primers and the expected band sizes for PCR are listed in Supplementary Table 1. Sample size was precalculated based on estimated variations to ensure adequate power. Experimental mice were randomly grouped, and experiments were set up and analyzed in a blind manner whenever possible.

Tamoxifen and BrdU treatment

Tamoxifen (Sigma-Aldrich, St. Louis, MO) was dissolved in corn oil and administrated i.p. into experimental mice at the age of 8 weeks (9 mg/40 g/day for four consecutive days unless otherwise specified). BrdU (Sigma-Aldrich, St. Louis, MO) (80 mg/kg) was administrated 1 day before mice were sacrificed.

Human specimens

Human peripheral zone (PZ) and transition zone (TZ) prostate specimens used in this study were obtained from patients undergoing prostatectomy for prostate cancer at the University of Washington with informed consent and Institutional Review Board (IRB) approval. IRB approval was obtained for medical record review to collect retrospective clinical and pathological data on each patient (IRB#2341). Peripheral zone tissues were obtained from patients with relatively smaller localized tumors (prostate weights between 25–35 g), and tissues were collected distant from major tumor nodules. Fresh specimens were fixed in 10% buffered formalin for 24 hours and processed for downstream analyses. Specimens were confirmed to be cancer free by H&E staining and immunostaining of *CK5* and *P63*.

Cell culture

8~12-week-old C57BL/6 mouse prostate tissues were collected, digested, and dissociated into single cells as described previously [38]. Dissociated single cells were cultured in Biocoat™ Collage I-coated plates (Corning, Corning, NY) in Bfs medium (5% Nu-Serum, 5% FBS, 1 × Insulin/Selenium, 1 × L-Glutamine, 1 × Penicillin/Streptomycin, and 1 × 10^{-10}M DHT in DMEM medium) at 37 °C with 5% CO_2. When the cell confluency reached around 90%, cells were trypsinized into single cells with 0.25% Trypsin-EDTA (Invitrogen, Carlsbad, CA). Cells were replated in Biocoat™ Collage I-coated plates (Corning, Corning, NY) for 30 min at 37 °C/5% CO_2. Unattached epithelial cells were discarded, and remaining stromal cells were cultured in Bfs media at 37 °C/5% CO_2 until 80–90% confluency. All the experiments in this study used fresh primary stromal cells within 3 weeks after single cell dissociation from prostates. WPMY-1, RM-1, and Pten-Kras cells were cultured in DMEM medium supplemented with 10% FBS and 1% penicillin/streptomycin at 37 °C/5% CO_2. WPMY-1 and RM1 were authenticated by STR Profiling annually and all cell lines were tested for mycoplasma contamination.

Tissue slice culture

Tissue slice culture was performed based on a previously published procedure [27]. Briefly, prostate tumor tissues were obtained from prostate cancer patients undergoing radical

prostatectomy. Tumor Gleason grading score and tumor stages of the five specimens we used are: 3 + 4/pT2, 3 + 4/pT2, 3 + 4/pT2, 3 + 4/pT3a, and 4 + 5/pT3b. Tissues were cut into slices of 200–300 μm using a Krumdieck Tissue Slicer and cultured in a well insert that is partially submerged in media and exposed to atmospheric oxygen. The tissues were cultured in advanced DMEM-F12 medium supplemented with 1% penicillin/streptomycin/Glutamax, 1x Amphotericin B, media supplements (components and sources of the supplement are listed in Supplementary Table 2) and 50 nM R1881 on a shaker in cell culture incubator at 37 °C/5% CO_2 with or without enzalutamide (10 μM).

Dissociation of mouse prostate and human prostate tissues

Prostate tissues were digested in DMEM/F12/Collagenase/Hyaluronidase/FBS (Invitrogen, Carlsbad, CA) for 3 hours at 37 °C, followed by an additional 1 hour of digestion in 0.25% Trypsin-EDTA (Invitrogen, Carlsbad, CA) on ice. Subsequently, digested cells were suspended in Dispase (Invitrogen, Carlsbad, CA, 5 mg/mL) and DNase I (Roche Applied Science, Indianapolis, IN, 1 mg/mL), and pipetted vigorously to dissociate cell clumps. Dissociated cells were then passed through 70 μm cell strainers (BD Biosciences, San Jose, CA) to get single cells.

Human prostate tissues were chopped into 2–3 mm-long pieces and incubated in 5 mg/ml collagenase type II/ advanced DMEM/F12 (1 ml per 50 mg of prostate tissue) with 10 μM of Y-27632 (STEMCELL technologies) for 5–12 hours. Tissues were pelleted, resuspended, and incubated in chilled 0.25% Trypsin-EDTA for 5 min. Thereafter, human prostate tissues were pelleted, resuspended in Dispase (Invitrogen, Carlsbad, CA, 5 mg/mL) and DNase I (Roche Applied Science, Indianapolis, IN, 1 mg/mL), and pipetted vigorously to dissociate cell clumps. Dissociated cells were then passed through 70 μm cell strainers (BD Biosciences, San Jose, CA) to obtain single cells.

Flow cytometry and cell sorting

Dissociated prostate or tumor cells were incubated with florescence conjugated antibodies at 4ºC for 30 minutes. Information for antibodies for FACS analyses and sorting is listed in Supplemental Table 3. FACS analyses and sorting were performed using BD LSR II, BD LSR Fortessa, and Aria III (BD Biosciences, San Jose, CA).

Plasmid and lentivirus production

Mouse C7 ORFs was purchased from Origene (Rockville, MD). 3x FLAG tag was PCR-incorporated at the N-terminus and subcloned into FUGW lentiviral vector at XbaI site for constitutive expression or subcloned into pCW57.1 lentiviral vector (a gift from Dr. David Root) at *NheI* and *SalI* sites for tet-inducible overexpression. Lentivirus preparation, titration, and infection of mouse prostate stromal cells or mouse cancer cell lines were performed as described previously [39]. Mouse C7 cDNA were amplified from mouse prostate stromal cells, FLAG tagged at C-terminus, fully sequenced, and cloned using the following primers: 5′- CGGCTAGCGC-CACCATGCAGGTGACAAGCTT 3′ and 5′- GCTAGCCTACTTGTCATCGT-CATCCTTGTAGTCGATGTCATGATCTTTATAATCACCGTCATGGTCTTTG-TAGTCCTGGGCTGCTTCTTCTGT 3′. The inducible ORF was

cloned from FUGW-C7 plasmid, and the forward primer was shared, and the reverse primer is 5′- GGGGACCACTTTGTACAAGAAAGCTGGGTtGTCGACCTACTTGT-CATCGTCATC 3′.

RNA purification and quantitative PCR (qPCR) analysis

Total RNA was extracted using NucleoSpin RNA Plus kit (Macherey-Nagel, Bethlehem, PA) and was then reverse transcribed with an iScript cDNA Synthesis Kit (Bio-Rad, Hercules, CA). Primers used in the qPCR experiments are listed in Supplementary Table 4. cDNA was analyzed by qPCR using the SYBR Green Gene Expression Assays (Bio-Rad, Hercules, CA), and data were normalized to *Gapdh* or *GAPDH*. Real-time PCR and data collection were performed on a QuantStudio5 Real-Time PCR system (Applied Biosystems, Foster City, CA).

qRT-PCR from Laser captured frozen tissues

Slides of 6 μm were sectioned from frozen blocks of human specimens using a Leica CM 1950 microtome, mounted onto Arcturus PEN Membrane Frame Slides (Thermo Scientific, Waltham, MA), fixed with 95% ethanol, and stained with Cresyl Violet (Acros Organic,New Jersey, NJ). Adjacent sections of 5 μm were cut and stained with hematoxylin and eosin. Histology review and slide annotation was performed by Martine Roudier. Areas of benign and Gleason patterns were marked if present. Areas of stroma and tumors were captured using the Arcturus XT (Thermo Scientific, Waltham, MA) with CapSure Macro LCM Caps (Thermo Scientific, LCM0211) and RNA was extracted using the Arcturus PicoPure RNA Isolation kit (Thermo Scientific, Waltham, MA) according to manufacturer's recommendations. RNA quality (DV200) and quantity were assessed using the Tape Station 4200 (Agilent Technologies, Santa Clara, CA) with High Sensitivity RNA Screen tape (Agilent Technologies, Santa Clara, CA). RNA was reverse transcribed to cDNA using iScript™ Reverse Transcriptase kit (BioRad, Hercules, CA). cDNA was preamplified using SsoAdvanced™ PreAmp Supermix (BioRad, Hercules, CA). qRT-PCR was performed using iTaq Universal SYBR Green Supermix (BioRad, Hercules, CA) and detected on a Quantstudio Real- Time PCR system (Applied Biosystems, Foster City, CA).

ChIP (Chromatin immunoprecipitation) - qPCR assay

Cells were crosslinked in cell culture media containing 1% formaldehyde for 10 minutes at room temperature. Cross-linking was terminated by adding 125 mM Glycine and rocking for 5 minutes at room temperature. Cells were harvested in PBS containing protease inhibitors (GenDEPOT, # P3100-001) and 1 mM PMSF. Subsequently, cells were centrifuged and resuspended in cell lysis buffer and sonicated using a bioruptor (Diagenode Inc., Denville NJ). Input samples were taken following sonication. ChIP was carried out using 4 μg antibodies against AR (sc-7305, Santa Cruz Biotech, Santa Cruz, CA) or normal mouse IgG (sc-2025, Santa Cruz Biotech, Santa Cruz, CA), respectively, and protein A/G beads slurry (Pierce UltraLink Immobilized Protein A/G, cat# PI-53133) overnight at 4 °C in siliconized tubes. Beads were collected and washed with low salt wash buffer (20 mM Tris-Cl pH 8.0, 150 mM NaCl, 2 mM EDTA, 1% Trition X 100, 0.1% SDS), High salt wash buffer (20 mM Tris-Cl pH 8.0, 500 mM NaCl, 2 mM EDTA, 1% Trition X 100, 0.1% SDS) and LiCl wash buffer (20 mM Tris, pH 8.0, 250 mM LiCl, 1 mM EDTA, 1% NP40,

1% Na-deoxycholate), respectively. Beads were then resuspended in elution buffer (50 mM $NaHCO_3$ and 1% SDS) for 15 minutes at room temperature. Formaldehyde crosslinks were reversed by incubating samples in reverse cross-linking buffer (0.3 M NaCl) at 65 °C for 2.5 hours. Remaining proteins and RNA were digested with Proteinase K (50 μg/μl) and RNase (0.1 mg/ml), respectively, at 37 °C for 1 hour. DNA was then isolated using the Purelink Quick Gel Extraction Kit (Invitrogen, Carlsbad, CA). qRT-PCR was performed to determine enrichment using the primers listed in Supplementary Table 5. Ct values from α-IgG and α-AR were normalized against Ct values generated from the input samples. The resulting value was then normalized by dilution and concentration to determine the value relative to the input.

Luciferase reporter assay

A 2 Kb genomic sequences upstream of the transcription start site of mouse *C7* containing 4 putative AR binding sites and human *C7* containing 2 putative AR binding sites were PCR amplified from the genomic DNA of mouse primary stromal cells and human 293 T cells, respectively, and cloned into the pGL3 luciferase vector (Promega, Madison, WI), generating the mouse and human pGL3-*C7*-luciferase reporters. The mouse amplicon was cloned into the vector via the *NheI* restriction site, and the human amplicon was cloned into the vector via the *KpnI* and *BglII* restriction sites upstream of luciferase. Mutations at the AR binding sites were performed by site-directed-mutagenesis using the Q5® Site-Directed Mutagenesis kit (New England Lab, Woburn, MA). The primers used in the construct cloning were listed in Supplementary Table 6. Cells were seeded in 6 well plates and co-transfected with 40 ng of pRL-CMV *Renilla* and 2 μg of pGL3-*C7*-luc or corresponding mutant constructs, respectively, using lipofectamine 3000 according to the manufacturer's instructions. 24 hours later, cells were infected with either FUCGW or FU-AR-CGW [40]. Two days later, luciferase activity was measured using the dual-luciferase reporter assay system (Promega, Madison, WI). Firefly luciferase activity was normalized to CMV-Renilla luciferase activity. Data were presented relative to CMV-Renilla readings and shown as mean ± s.d. Experiments were performed in triplicates.

Western blots

Cells or tissues were lysed in RIPA buffer (20 mM Tris-HCl, pH 7.5, 150 mM NaCl, 1 mM Na2EDTA, 1 mM EGTA, 1% NP-40, 1% sodium deoxycholate, 2.5 mM sodium pyrophosphate, 1 mM β-glycerophosphate, 1 mM Na_3VO_4) supplemented with protease cocktail inhibitors (GenDEPOT, # P3100-001) and phosphatase inhibitors (GenDEPOT, # P3200-005). The protein concentration was measured using the by a Bradford Assay kit (BioRad, Hercules, CA). Western blot analysis was performed with precast gradient gels (4–12%) (GenScript, SurePage # M00654) using standard methods. Proteins were separated by SDS-PAGE and transferred onto a nitrocellulose membrane (0.2 μm. Bio-Rad). Membranes were blocked in 5% BSA in PBST for 1 hour at room temperature, and then incubated with the specific primary antibodies overnight at 4 °C, washed in PBST, incubated with an HRP-conjugated secondary antibody (Jackson ImmunoResearch, Inc., West Grove, PA) for 1 hour at room temperature, and developed by the ECL reagent (Thermal Scientific, Rockford, IL). The bands were visualized by chemiluminescence (Amersham Imager 600). The following antibodies were used: antibodies against Flag (F1804 Sigma), cleavage-caspase 3 (CST,

9661 S), AR (441, Santa Cruz), and β-actin (A2228, sigma, mouse). The ImageJ program was used for densitometric analysis of western blots, and the quantification results were normalized to an internal control.

Histology and immunostaining

Tissues were fixed in 10% buffered formalin and paraffin embedded. H&E staining and immunofluorescence staining were performed with 5 μm sections. For hematoxylin and eosin staining and immunostaining, sections were processed as described previously. For immunostaining, sections were processed as described previously [41] and incubated with primary antibody in 3% of normal goat serum (Vector Laboratories, Burlingame, CA) overnight. Slides then were incubated with secondary antibodies (diluted 1:250 in PBST) labeled with Alexa Fluor 488 and/or 594 (Invitrogen/Molecular Probes, Eugene, OR). Sections were counterstained with either hematoxylin or 4,6-diamidino-2-phenylindole (DAPI) (Sigma-Aldrich, St. Louis, MO). Immunofluorescence staining was imaged using a Leica SP8 fluorescence microscope or a Leica EL6000 confocal microscope (Leica Microsystems, Wetzlar, Germany). The following antibodies were used: antibodies against BrdU (abcam, ab6326, Rat), K5 (905501, Biolegend, Rabbit), K8 (Covance, MMS-162P/1E8, Mouse) and C5b-9 (WU13-15, ab55811, Abcam).

Statistical analyses

Data are presented as means ± s.d. Student's t test and one-way or two-way ANOVA with multiple comparisons were used to determine significance in two-group and multiple-group experiments, respectively. For all statistical tests, the two-tail $p \leq 0.05$ level of confidence was accepted for statistical significance.

Supplementary Material

Refer to Web version on PubMed Central for supplementary material.

ACKNOWLEDGEMENTS

We thank the patients and their families for supporting this research, Brenda Nghiem and Lori Kollath for sample identification and processing, and Dr. Xiaomu Zhang for maintaining the C7 mice. This work is supported by W81XWH-20-1-0218 (L.X.), R01CA190378 (L.X.), the Pritt Family Endowment, P50CA97186, P01CA163227, and the Institute for Prostate Cancer Research (IPCR).

FUNDING

DoD, NCI.

DATA AVAILABILITY

All data generated or analyzed during this study are included in this published article and its supplementary information files.

REFERENCES

1. Watson PA, Arora VK, Sawyers CL. Emerging mechanisms of resistance to androgen receptor inhibitors in prostate cancer. Nat Rev Cancer 2015;15:701–11. [PubMed: 26563462]

2. Ricklin D, Reis ES, Lambris JD. Complement in disease: a defence system turning offensive. Nat Rev Nephrol 2016;12:383–401. [PubMed: 27211870]
3. Revel M, Daugan MV, Sautes-Fridman C, Fridman WH, Roumenina LT. Complement system: promoter or suppressor of cancer progression? Antibodies 2020;9:57. [PubMed: 33113844]
4. Rutkowski MJ, Sughrue ME, Kane AJ, Mills SA, Parsa AT. Cancer and the complement cascade. Mol Cancer Res 2010;8:1453–65. [PubMed: 20870736]
5. Reis ES, Mastellos DC, Ricklin D, Mantovani A, Lambris JD. Complement in cancer: untangling an intricate relationship. Nat Rev Immun 2018;18:5–18.
6. Loberg RD, Day LL, Dunn R, Kalikin LM, Pienta KJ. Inhibition of decay-accelerating factor (CD55) attenuates prostate cancer growth and survival in vivo. Neoplasia 2006;8:69–78. [PubMed: 16533428]
7. Xu C, Jung M, Burkhardt M, Stephan C, Schnorr D, Loening S, et al. Increased CD59 protein expression predicts a PSA relapse in patients after radical prostatectomy. Prostate 2005;62:224–32. [PubMed: 15389793]
8. July LV, Akbari M, Zellweger T, Jones EC, Goldenberg SL, Gleave ME. Clusterin expression is significantly enhanced in prostate cancer cells following androgen withdrawal therapy. Prostate 2002;50:179–88. [PubMed: 11813210]
9. Tschopp J, Chonn A, Hertig S, French LE. Clusterin, the human apolipoprotein and complement inhibitor, binds to complement C7, C8 beta, and the b domain of C9. J Immunol 1993;151:2159–65. [PubMed: 8345200]
10. Emin M, Wang G, Castagna F, Rodriguez-Lopez J, Wahab R, Wang J, et al. Increased internalization of complement inhibitor CD59 may contribute to endothelial inflammation in obstructive sleep apnea. Sci Transl Med 2016;8:320ra1.
11. Wurzner R Modulation of complement membrane attack by local C7 synthesis. Clin Exp Immun 2000;121:8–10. [PubMed: 10886232]
12. Wurzner R, Joysey VC, Lachmann PJ. Complement component C7. Assessment of in vivo synthesis after liver transplantation reveals that hepatocytes do not synthesize the majority of human C7. J Immunol 1994;152:4624–9. [PubMed: 8157976]
13. Fosbrink M, Niculescu F, Rus H. The role of c5b-9 terminal complement complex in activation of the cell cycle and transcription. Immun Res 2005;31:37–46.
14. Triantafilou K, Hughes TR, Triantafilou M, Morgan BP. The complement membrane attack complex triggers intracellular Ca2+ fluxes leading to NLRP3 inflammasome activation. J Cell Sci 2013;126:2903–13. [PubMed: 23613465]
15. Bossi F, Rizzi L, Bulla R, Debeus A, Tripodo C, Picotti P, et al. C7 is expressed on endothelial cells as a trap for the assembling terminal complement complex and may exert anti-inflammatory function. Blood 2009;113:3640–8. [PubMed: 19179470]
16. Wang S, Hu W, Xie Y, Wu H, Jia Z, Zhang Z, et al. Functional genetic variants in complement component 7 confer susceptibility to gastric cancer. PeerJ 2022;10:e12816. [PubMed: 35111412]
17. Ying L, Zhang F, Pan X, Chen K, Zhang N, Jin J, et al. Complement component 7 (C7), a potential tumor suppressor, is correlated with tumor progression and prognosis. Oncotarget 2016;7:86536–46. [PubMed: 27852032]
18. Tyekucheva S, Bowden M, Bango C, Giunchi F, Huang Y, Zhou C, et al. Stromal and epithelial transcriptional map of initiation progression and metastatic potential of human prostate cancer. Nat Commun 2017;8:420. [PubMed: 28871082]
19. Kwon OJ, Zhang Y, Li Y, Wei X, Zhang L, Chen R, et al. Functional heterogeneity of mouse prostate stromal cells revealed by single-cell RNA-Seq. iScience 2019;13:328–38. [PubMed: 30878879]
20. Joseph DB, Henry GH, Malewska A, Reese JC, Mauck RJ, Gahan JC, et al. Single-cell analysis of mouse and human prostate reveals novel fibroblasts with specialized distribution and microenvironment interactions. J Pathol 2021;255:141–54. [PubMed: 34173975]
21. Wei X, Roudier MP, Kwon OJ, Lee JD, Kong K, Dumpit R, et al. Paracrine Wnt signaling is necessary for prostate epithelial proliferation. Prostate 2022;82:517–30. [PubMed: 35014711]

22. Wei X, Zhang L, Zhou Z, Kwon OJ, Zhang Y, Nguyen H, et al. Spatially restricted stromal wnt signaling restrains prostate epithelial progenitor growth through direct and indirect mechanisms. Cell Stem Cell 2019;24:753–68.e6. [PubMed: 30982770]
23. Jia D, Zhou Z, Kwon OJ, Zhang L, Wei X, Zhang Y, et al. Stromal FOXF2 suppresses prostate cancer progression and metastasis by enhancing antitumor immunity. Nat Commun 2022;13:6828. [PubMed: 36369237]
24. Wei X, Zhang L, Zhang Y, Cooper C, Brewer C, Tsai CF, et al. Ablating Lgr5-expressing prostatic stromal cells activates the ERK-mediated mechanosensory signaling and disrupts prostate tissue homeostasis. Cell Rep 2022;40:111313. [PubMed: 36070687]
25. Sboner A, Demichelis F, Calza S, Pawitan Y, Setlur SR, Hoshida Y, et al. Molecular sampling of prostate cancer: a dilemma for predicting disease progression. BMC Med Genomics 2010;3:8. [PubMed: 20233430]
26. Taylor BS, Schultz N, Hieronymus H, Gopalan A, Xiao Y, Carver BS, et al. Integrative genomic profiling of human prostate cancer. Cancer Cell 2010;18:11–22. [PubMed: 20579941]
27. Maund SL, Nolley R, Peehl DM. Optimization and comprehensive characterization of a faithful tissue culture model of the benign and malignant human prostate. Lab Investig 2014;94:208–21. [PubMed: 24296879]
28. Berman-Booty LD, Sargeant AM, Rosol TJ, Rengel RC, Clinton SK, Chen CS, et al. A review of the existing grading schemes and a proposal for a modified grading scheme for prostatic lesions in TRAMP mice. Toxicol Pathol 2012;40:5–17. [PubMed: 22021166]
29. Beltran H, Hruszkewycz A, Scher HI, Hildesheim J, Isaacs J, Yu EY, et al. The role of lineage plasticity in prostate cancer therapy resistance. Clin Cancer Res 2019;25:6916–24. [PubMed: 31363002]
30. Gonzalez S, Martinez-Borra J, Lopez-Larrea C. Cloning and characterization of human complement component C7 promoter. Genes Immun 2003;4:54–9. [PubMed: 12595902]
31. Erbersdobler A, Augustin H, Schlomm T, Henke RP. Prostate cancers in the transition zone: Part 1; pathological aspects. BJU Int 2004;94:1221–5. [PubMed: 15610093]
32. Krieger JN, Ross SO, Riley DE. Chronic prostatitis: epidemiology and role of infection. Urology 2002;60:8–12.
33. Nash C, Boufaied N, Badescu D, Wang YC, Paliouras M, Trifiro M, et al. Genome-wide analysis of androgen receptor binding and transcriptomic analysis in mesenchymal subsets during prostate development. Dis Models Mech 2019;12:dmm039297.
34. Zhang J, Gonit M, Salazar MD, Shatnawi A, Shemshedini L, Trumbly R, et al. C/EBPalpha redirects androgen receptor signaling through a unique bimodal interaction. Oncogene 2010;29:723–38. [PubMed: 19901962]
35. Leach DA, Panagopoulos V, Nash C, Bevan C, Thomson AA, Selth LA, et al. Cell-lineage specificity and role of AP-1 in the prostate fibroblast androgen receptor cistrome. Mol Cell Endocrinol 2017;439:261–72. [PubMed: 27634452]
36. Kwon OJ, Zhang B, Jia D, Zhang L, Wei X, Zhou Z, et al. Elevated expression of the colony-stimulating factor 1 (CSF1) induces prostatic intraepithelial neoplasia dependent of epithelial-Gp130. Oncogene 2022;41:1309–23. [PubMed: 34999736]
37. De Gendt K, Swinnen JV, Saunders PT, Schoonjans L, Dewerchin M, Devos A, et al. A Sertoli cell-selective knockout of the androgen receptor causes spermatogenic arrest in meiosis. Proc Natl Acad Sci USA 2004;101:1327–32. [PubMed: 14745012]
38. Valdez JM, Zhang L, Su Q, Dakhova O, Zhang Y, Shahi P, et al. Notch and TGFbeta form a reciprocal positive regulatory loop that suppresses murine prostate basal stem/progenitor cell activity. Cell Stem Ccell 2012;11:676–88.
39. Kwon OJ, Zhang L, Jia D, Zhou Z, Li Z, Haffner M, et al. De novo induction of lineage plasticity from human prostate luminal epithelial cells by activated AKT1 and c-Myc. Oncogene 2020;39:7142–51. [PubMed: 33009488]
40. Xin L, Teitell MA, Lawson DA, Kwon A, Mellinghoff IK, Witte ON. Progression of prostate cancer by synergy of AKT with genotropic and nongenotropic actions of the androgen receptor. Proc Natl Acad Sci USA 2006;103:7789–94. [PubMed: 16682621]

41. Choi N, Zhang B, Zhang L, Ittmann M, Xin L. Adult murine prostate basal and luminal cells are self-sustained lineages that can both serve as targets for prostate cancer initiation. Cancer Cell 2012;21:253–65. [PubMed: 22340597]

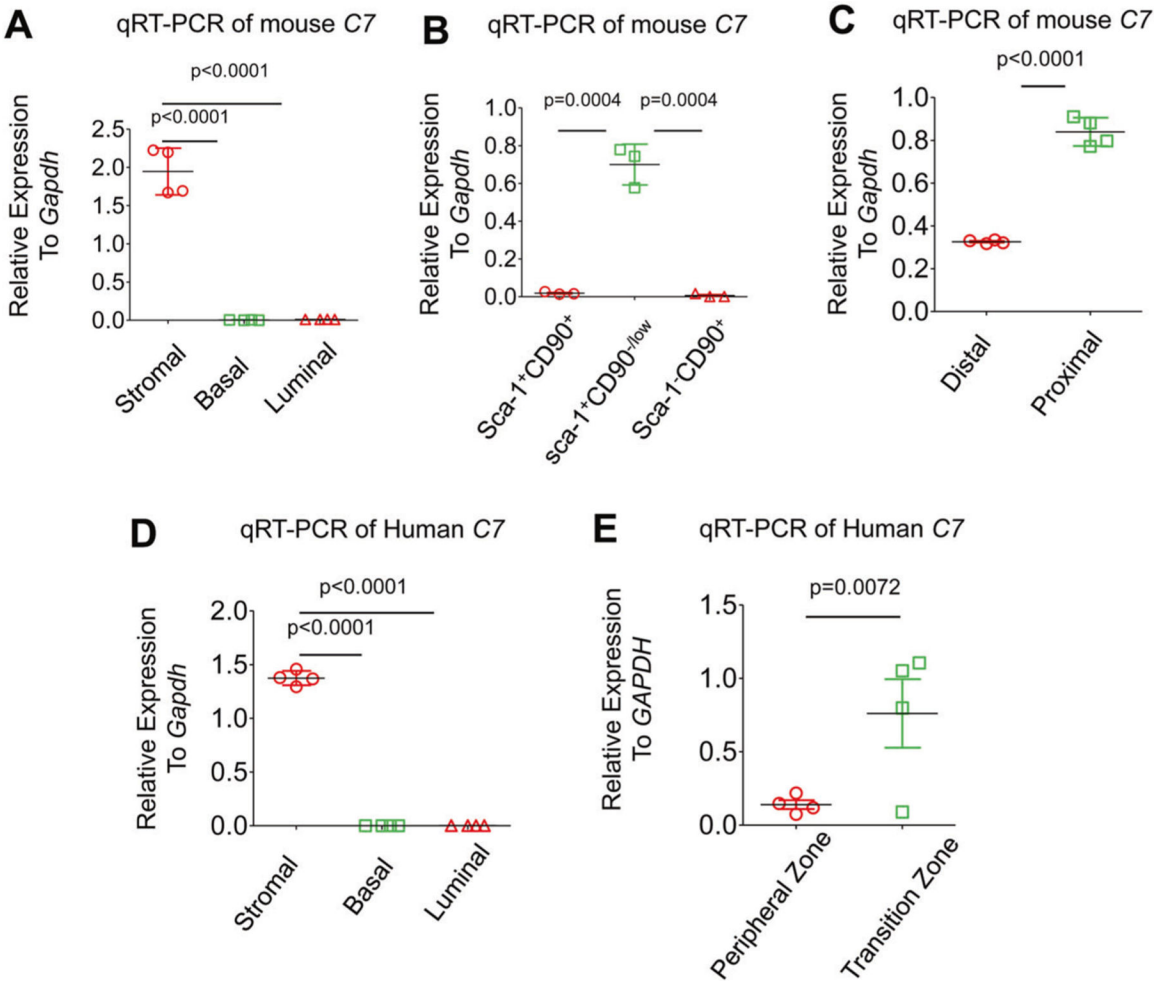

Fig. 1. *C7* is expressed by stromal cells in mouse and human prostates.

A qRT-PCR of *C7* in FACS-separated mouse prostate cell lineages. Dot plot shows ± s.d. from 4 experiments. **B** qRT-PCR analysis of *C7* in FACS-isolated prostate stromal subpopulations. Dot plot shows ± s.d. from 3 experiments. **C** qRT-PCR analysis of *C7* in FACS-isolated mouse proximal and distal prostate stromal cells. Data represent means ± s.d. from 4 independent experiments. **D** qRT-PCR analysis of *C7* in FACS-isolated human prostate cell lineages. Data represent means ± s.d. from 4 independent experiments. **E** qRT-PCR analysis of human *C7* in FACS-isolated stromal cells from human peripheral and transition prostate zones. Data represent means ± s.d. from 4 independent experiments.

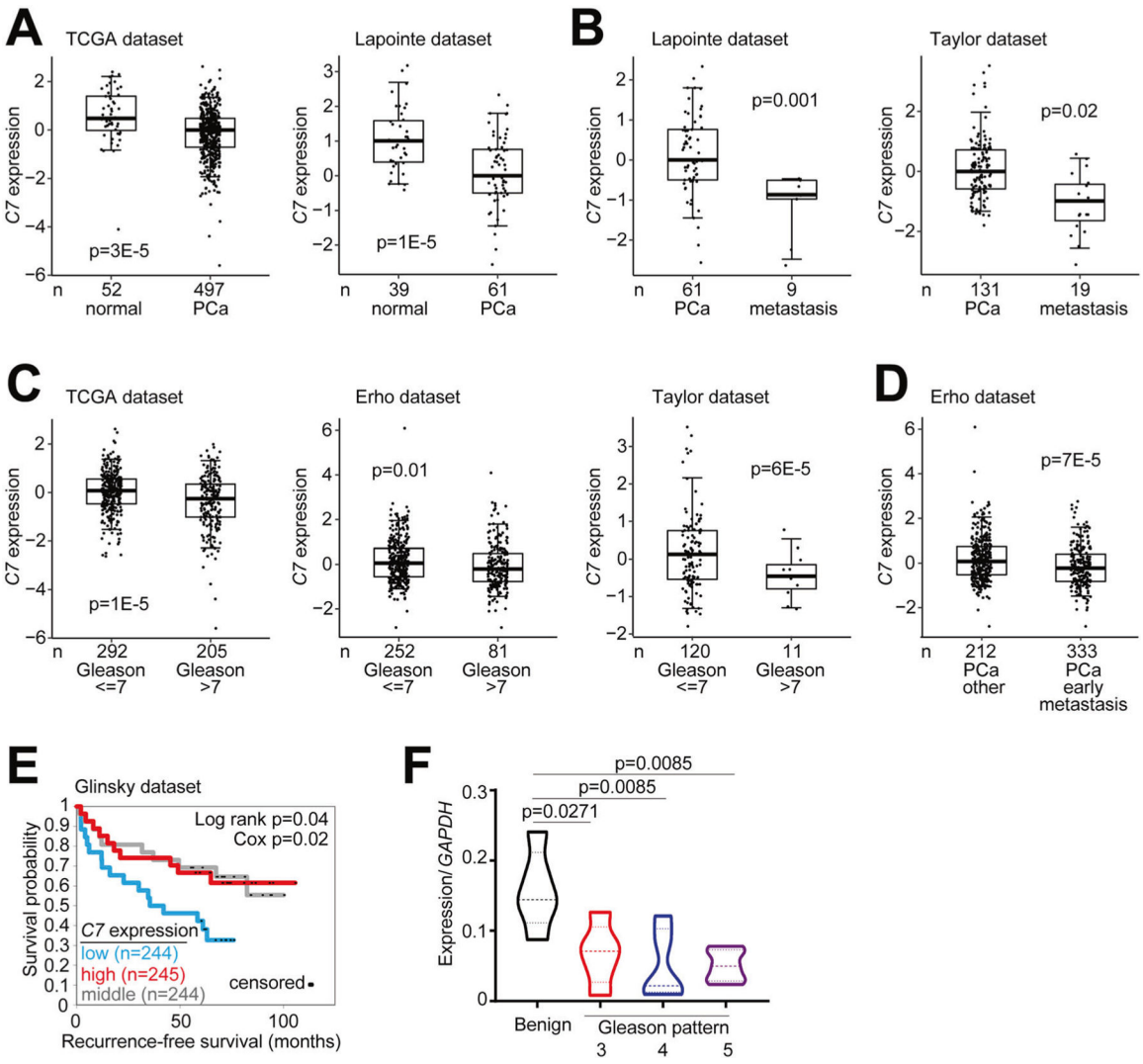

Fig. 2. Stromal C7 expression inversely correlates with prostate cancer progression.

A Box plots show *C7* expression in prostate cancer specimens and normal tissues from two prostate datasets. **B** Box plot shows *C7* expression in metastatic prostate cancer specimens and primary prostate cancer specimens in 2 prostate cancer datasets. **C** Box plots show that *C7* expression correlations with Gleason scores in three human prostate cancer datasets. **D** Box plot shows a correlation of *C7* expression with early metastasis after rising PSA in the Erho dataset. For parts (**a–d**), Boxplot P-values by heteroscedastic t-test. Box plots represent 5% (lower whisker), 25% (lower box), 50% (median), 75% (upper box), and 95% (upper whisker). **E** Kaplan-Meier plot for correlations of *C7* expression with prostate cancer biochemical recurrence in the Glinsky dataset. Log-rank test: $p = 0.04$. Univariate Cox (treating C7 expression as a continuous variable): $p = 0.02$. **F** Expression of *C7* in laser-captured stromal cells from prostate cancer of different Gleason patterns and adjacent benign tissues by qRT-PCR. Each dot in plot represents value calculated from one laser captured specimen. Data show values collected from 20 laser-captured samples from 13 prostate cancer specimens, analyzed by one-way ANOVA with Turkey's multiple comparison test.

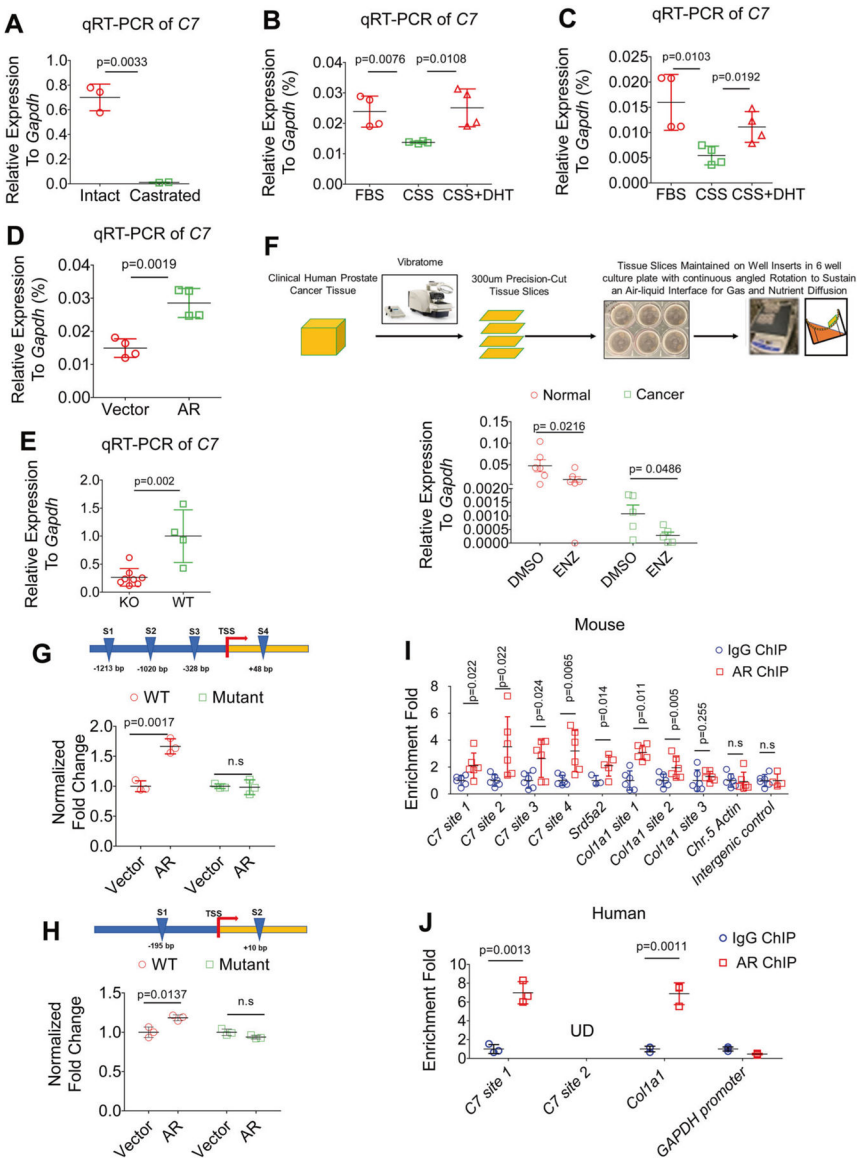

Fig. 3. C7 is regulated by androgen receptor signaling.

A qRT-PCR analysis of *C7* in FACS-isolated stromal cells from intact and castrated mice. Dot plot shows means ± s.d. from 3 intact and 2 castrated mice. **B, C** qRT-PCR analysis of *C7* in embryonic urogenital sinus mesenchymal cells (**B**) and primarily cultured adult mouse prostate stromal cells (**C**) grown with fetal bovine sera, charcoal striped sera (CSS), and CSS supplemented with 10 nM dihydrotestosterone (DHT). Data represent means ± s.d. from 4 independent experiments. **D** qRT-PCR analysis of *C7* in primarily adult mouse prostate stromal cells with or without ectopic AR expression. Data represents means ± s.d. from 4 independent experiments. **E** qRT-PCR analysis of *C7* in FACS-isolated stromal cells from 12-wk-old C57Bl/6 wildtype (WT) and littermate Col1a2-CreER^{T2};AR$^{Flox/Y}$ (KO) mice at 1 month after treatment with tamoxifen. Each dot represents data from one mouse. N = 4 for WT and N = 8 for KO group. **F** Schematic illustration of experimental design for tissue slice culture. Bottom dot plot shows qRT-PCR analysis of *C7* in benign tissues and

prostate cancer specimens cultured with or without enzalutamide. Each dot represents data from one patient specimen. N = 6 for benign group and N = 5 for prostate cancer specimen. Luciferase assays determine activity of mouse (**G**) and human (**H**) C7 promoter reporter with and without mutations of all putative AR binding sites in control and AR-expressing mouse prostate stromal cells (**G**) and WPMY cells (**H**). Data represent means ± s.d. N = 3. TSS: transcription start site. I ChIP analysis of AR binding at *C7* promoter in mouse prostate stromal cells. Dot plot shows means ± s.d. of relative enrichment from 3 independent experiments. Loci at Ch.5 and intergenic control serve as negative and *Srd5a2* serves as positive control. J ChIP analysis of AR binding at *C7* promoter in human WPMY-1 cells. Dot plot shows means ± s.d. of relative enrichment. *GAPDH* and *COL1A1* serve as negative and positive controls, respectively. UD undetectable.

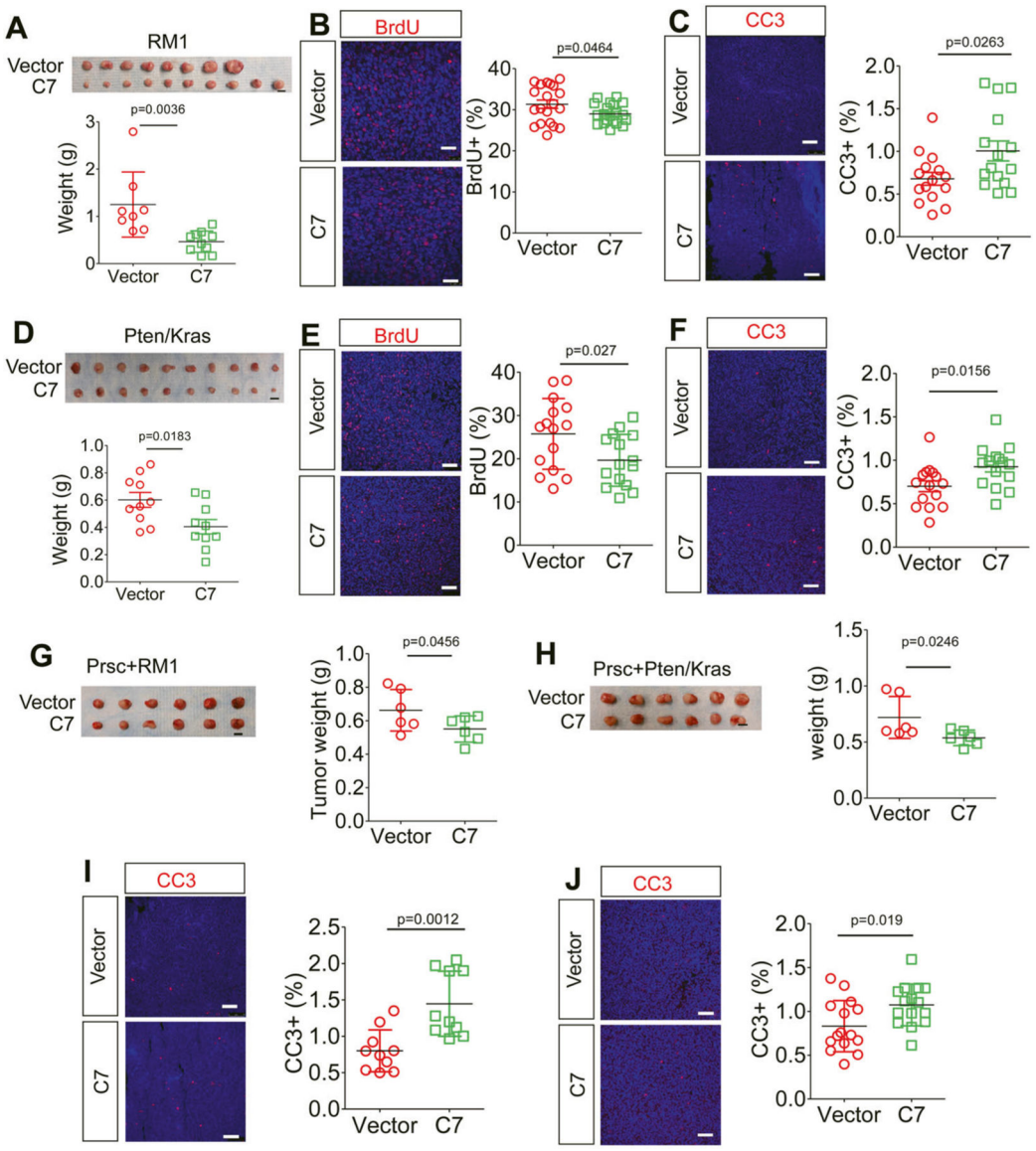

Fig. 4. C7 suppresses prostate tumor growth in vivo.

A Image of subcutaneous RM-1 tumors with and without C7 overexpression. Dot plot shows means ± s.d. of tumor weight. N = 8 for control group and N = 10 for C7 overexpression group. Statistical analysis by Student's t-test. Scale bar = 1 cm. Immunostaining of BrdU (**B**) and CC3 (**C**). Dot plots show means ± s.d. of $BrdU^+$ and $CC3^+$ cells. Individual dots represent results from 15 random images from 5 different tumors per group. Scale bars = 75 μm. **D** Image of subcutaneous *Pten-Kras* tumors with or without C7 overexpression. Dot plot shows means ± s.d. of tumor weight. N = 10 for each group. Statistical analysis by Student's t-test. Scale bar = 1 cm. Immunostaining of BrdU (**E**) and CC3 (**F**). Dot plots show means ± s.d. of $BrdU^+$ and $CC3^+$ cells. Individual dots represent results from 15 random images from 5 different tumors per group. Scale bars = 75 μm. **G** Image of RM-1 tumors grown subcutaneously with control (Vector) and C7-expressing mouse prostate stromal cells. Dot plot shows means ± s.d. of tumor weight. Bar = 1 cm. N = 6 tumors per group. One-sided

unpaired t-test. **H** Image of *Pten-Kras* tumors grown subcutaneously with control (Vector) and C7-expressing mouse prostate stromal cells. Dot plot shows means ± s.d. of tumor weight. Bar = 1 cm. N = 6 tumors per group. One-sided unpaired t-test. **I** Immunostaining of CC3 of RM1 tumors. Scale bar= 75μm. Dot plots show means ± s.d. of $CC3^+$ cells. Individual dots represent data of 10 images from 5 tumors per group. **J** Immunostaining of CC3 of *Pten-Kras* tumors. Scale bar= 75μm. Dot plots show means ± s.d. of $CC3^+$ cells. Individual dots represent data of 10 images from 5 tumors per group.

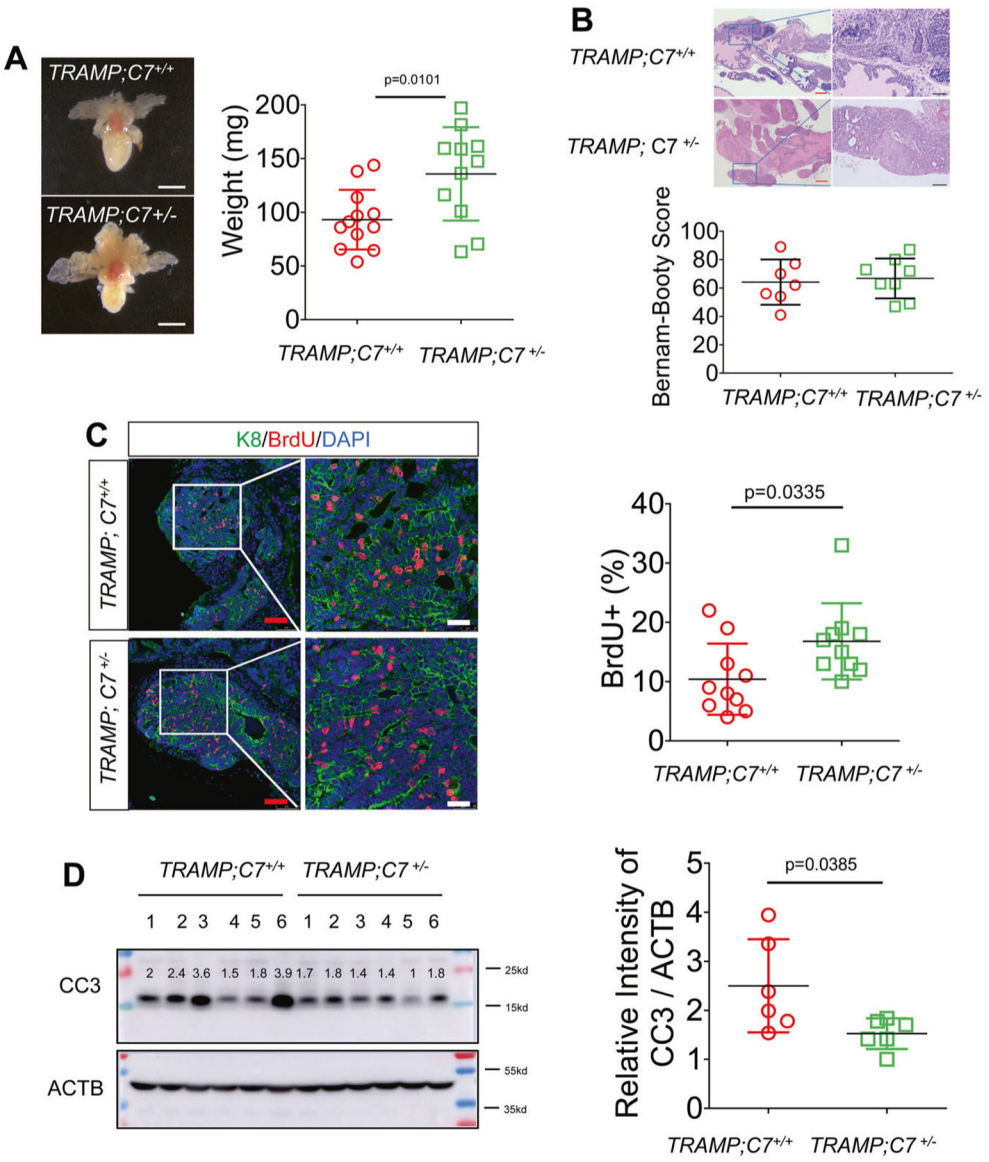

Fig. 5. C7 haploinsufficiency promotes tumor growth in *TRAMP* model.

A Transillumination images of prostates of 22-wk-old control (*TRAMP*) and *TRAMP;C7* $^{+/-}$ mice. Dot plot shows means ± s.d. of prostate weight. N = 12 for control and N = 11 for *TRAMP;C7* $^{+/-}$. Bars = 2 mm. **B** H&E staining of prostates of 22-wk-old control (*TRAMP*) and *TRAMP;C7* $^{+/-}$ mice. Red scale bars = 250 μm, black scale bar =75 μm. Dot plot shows Berman-Booty scores of histology. Each dot represents a score calculated from one tissue slide from one mouse. Scores were collected from 7 control and 8 *TRAMP;C7* $^{+/-}$. Statistical analysis by unpaired t-test. **C** Coimmunostaining of luminal cell marker Keratin 8 (K8) and BrdU. Dot plots show means ± s.d. of BrdU^{+} cells from 10 tumors per group. **D** Western blot analysis of CC3 in prostate tumors. Dot plots show means ± s.d. of relative CC3 intensity normalized by internal control (ACTB) intensity from 6 tumors per group. Statistical analysis by Student's t-test.

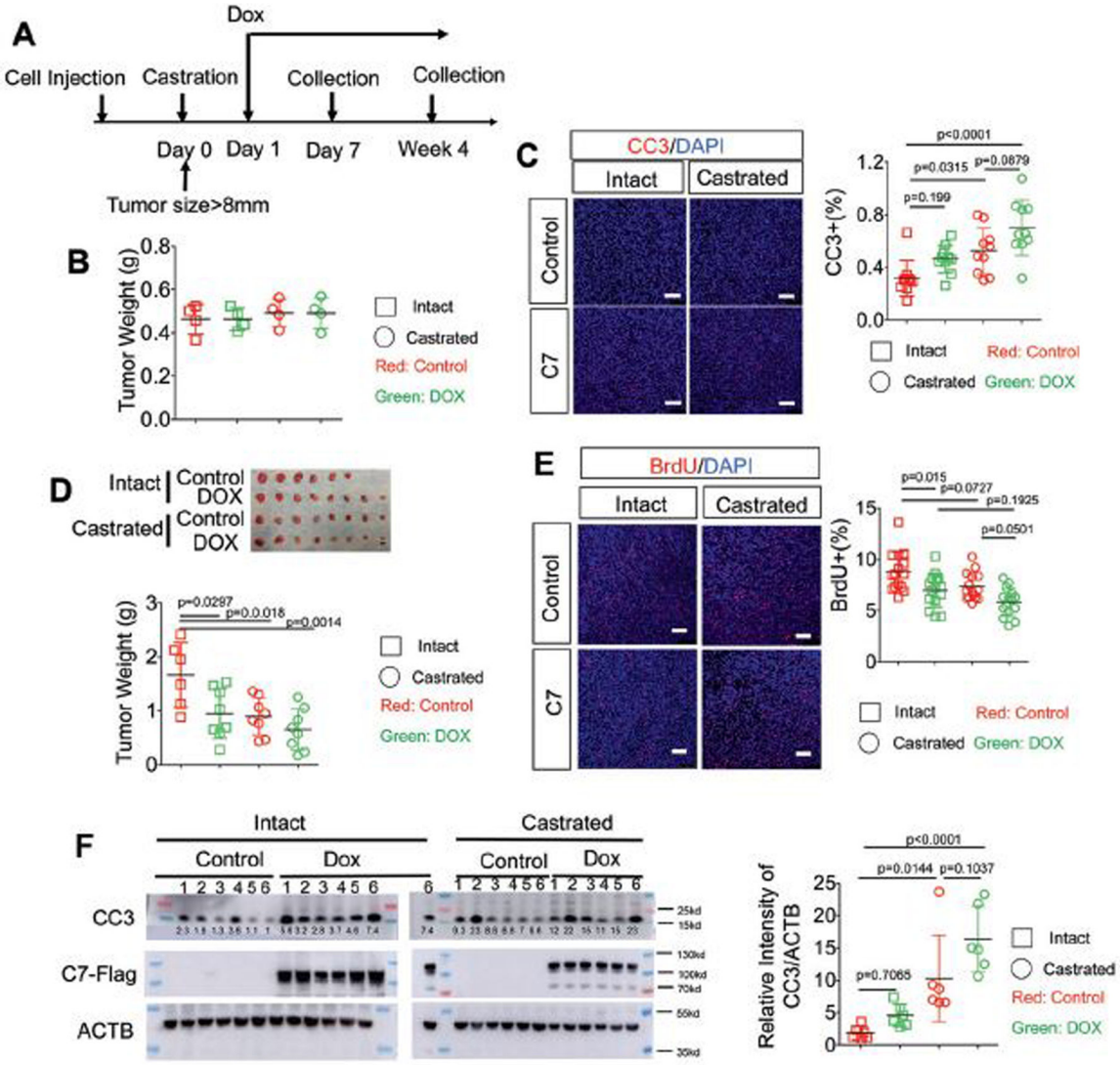

Fig. 6. Restoring C7 expression enhances the response of *Pten-Kras* to androgen deprivation.

A Schematic illustration of experimental design. DOX: doxycycline. **B** Dot plot shows means ± s.d. of prostate tumor weight at day 7 after Dox treatment. **C** Immunostaining of CC3. Dot plots show means ± s.d. of $CC3^+$ cells. Scale bars = 75 μm. **D** Image of *Pten-Kras* tumors at 4-weeks after Dox treatment. Dot plot shows means ± s.d. of tumor weight. Scale bar = 1 cm. **E** Immunostaining of BrdU. Dot plots show means ± s.d. of $BrdU^+$ cells. Scale bars = 75 μm. **F** Western blot analysis of CC3 in xenograft tumor samples. N = 6 per group. Dot plots shows means ± s.d. of relative CC3 intensity normalized by β-Actin expression. Sample #6 in Dox group of intact mice was included in gel on the right to serve as a control to normalize densitometric intensity. All statistical analyses by two-way ANOVA with Turkey's multiple comparison test.